Materials Transactions, Vol. 44, No. 10 (2003) pp. 1993 to 1998
Special Issue on Nano-Hetero Structures in Advanced Metallic Materials

Microstructure of Rapidly Solidified High Strength $Al_{94}V_4Fe_2$ Alloy

B. S. Murty[1]*, D. H. Ping[2], K. Hono[2], H. Kimura[3] and A. Inoue[3]

[1]*Indian Institute of Technology, Kharagpur 721 302, India*
[2]*National Institute for Materials Science, Tsukuba 305-0047, Japan*
[3]*Institute for Materials Research, Tohoku University, Sendai 980-8577, Japan*

$Al_{94}V_4Fe_2$ alloy melt-spun at different wheel velocities in the range of 20-50 m/s has been studied. The microstructure of the alloy consists of a nanoquasicrystalline phase in an Al matrix at slow cooling rates, while at higher cooling rates it shows nanodomains of an amorphous phase embedded in the Al matrix. The tensile fracture strength of the alloy reaches a maximum when it exhibits a nanocomposite microstructure consisting of quasicrystalline phase and Al. The composition of the quasicrystalline and amorphous phases has been identified using three dimensional atom probe field ion microscopy.

(Received May 14, 2003; Accepted July 24, 2003)

Keywords: *aluminium alloy, amorphous, quasicrystal, nanocrystal, transmission electron microscopy, 3 dimensional atom probe*

1. Introduction

Recently, a number of rapidly solidified high strength Al alloys containing nanocrystalline Al, amorphous and/or nanoquasicrystalline phases have been developed.[1–3] Among these the most popular ones are $Al_{88}Ni_9Ce_2Fe_1$ alloy[4,5] with nanosized Al grains in an amorphous matrix, $Al_{92}Mn_6Ce_2$[6] and $Al_{94.5}Cr_3Ce_1Co_{1.5}$ alloys[7] with nanocrystalline Al and nanoquasicrystalline phase mixture. Bulk icosahedral alloys such as $Al_{95}Fe_3Cr_2Ti_2$ alloy[8] with excellent elevated temperature strength have also been developed. In spite of these reports, the correlation between the microstructure and mechanical properties has not yet been clearly established so far in these high strength Al alloys.

Reports on the high strength $Al_{94}V_4Fe_2$ alloy[9–13] suggest that the phases present vary from a mixture of nanocrystalline Al and amorphous to nanocrystalline Al and quasicrystalline icosahedral phase (*i*-phase) mixture depending on the cooling rate during melt spinning. Thus, there is a possibility to establish the correlation between the microstructure and the mechanical properties in this alloy, if a detailed microstructural characterization is carried out as a function of cooling rate. Hono *et al.*[12] have done this for the $Al_{94}V_4Fe_2$ alloy containing nanoscale mixture of amorphous phase and fcc α-Al, but they did not confirm the presence of the *i*-phase in their sample. Using an energy compensated one-dimensional atom probe, Hono *et al.*[12] have also shown that the amorphous phase is enriched in Fe and V. Humphreys *et al.*[13] have analyzed the $Al_{94}V_4Fe_2$ alloy containing a nanoscale mixture of Al and *i*-phase with the help of an energy compensated three-dimensional atom probe and concluded that the *i*-phase is enriched in Fe and V.

However, both of the above reports have not attempted to correlate the strength of the alloys to the microstructure observed. The early works of Inoue *et al.* and others in Al based alloys[1] suggest that the best mechanical properties are achieved when the microstructure consists of a nanocomposite of Al and amorphous phase. The present paper attempts to clarify this point through a detailed microstructural analysis of the $Al_{94}V_4Fe_2$ alloy at different cooling rates. The present results are important in view of the ongoing alloy design efforts in the scientific community to develop high strength Al alloys.

*Corresponding author, E-mail: bsm@metal.iitkgp.ernet.in

2. Experimental Details

The $Al_{94}V_4Fe_2$ alloy was prepared by arc-melting high purity metals. The alloy ingot was remelted several times in order to achieve homogeneity in composition. The alloy was rapidly solidified by single roller melt spinning at wheel surface velocities ranging from 20-50 m/s. The thermal stability of the melt-spun alloys was studied by differential scanning calorimetry (DSC) at a heating rate of 0.67 K/s using a Perkin Elmer Pyris-I DSC. The x-ray diffraction (XRD) analysis was carried out using a Rigaku x-ray diffractometer (RINT 2500) with CuK_α radiation. Transmission electron microscopy (TEM) was performed using a Philips CM20 and high resolution electron microscopy (HREM) with a JEOL JEM-4000EX. The samples for TEM observation were prepared by ion milling by maintaining the specimen at -30°C using liquid nitrogen. The tensile tests were carried out using Instron testing machine at a strain rate of $8.3 \times 10^{-4}\,s^{-1}$ with the specimens of 0.7 mm width and 0.02 mm thickness and a gauge length of 10 mm. The atomic distribution in the alloy, on the nanoscale, was characterized using an energy compensated three dimensional atom probe (3DAP) equipped with the CAMECA optical tomographic atom probe detection system.[14]

3. Results

Figure 1 shows the XRD patterns of the $Al_{94}V_4Fe_2$ alloy at different melt-spun wheel velocities in the range of 20-50 m/s. The alloy melt-spun at 20 m/s showed a mixture of α-Al and *i*-phase. With an increase in wheel velocity (cooling rate) up to 40 m/s, the XRD peaks of *i*-phase became broader and less intense suggesting refinement of its particle size. At 50 m/s, the peaks of *i*-phase were replaced with a broad peak indicating the formation of the amorphous phase at this cooling rate.

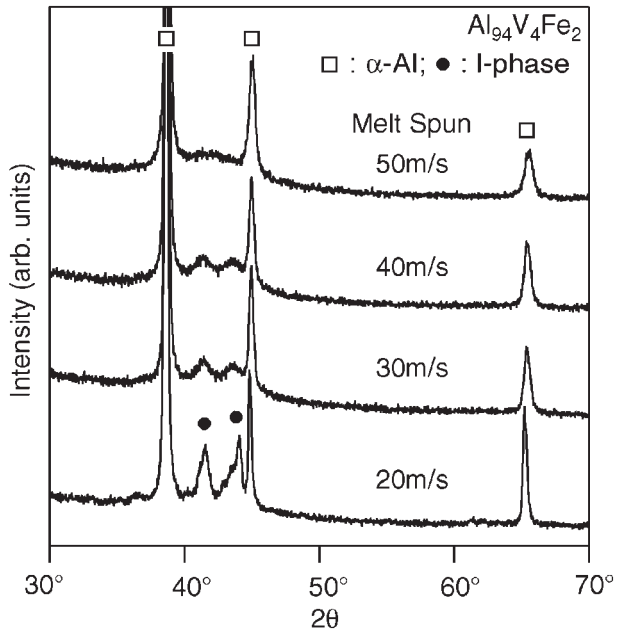

Fig. 1 XRD patterns of $Al_{94}V_4Fe_2$ alloy melt-spun in the wheel velocity range of 20-50 m/s.

Figures 2(a) and (b) show the TEM bright field images of the alloy melt-spun at 20 and 50 m/s, respectively. The alloy melt-spun at 20 m/s showed the presence of spherical nanoscale *i*-phase particles in an α-Al matrix, with their particle size ranging from about 10-80 nm. The microdiffraction pattern obtained from one of these particles (inset of Fig. 2(a)) shows the 5-fold orientation confirming its quasicrystalline nature.

The alloy melt-spun at 50 m/s showed nanocrystalline fcc α-Al grains of about 50-100 nm in an amorphous matrix as shown in Fig. 2(b). The selected area diffraction pattern obtained from this alloy (inset of Fig. 2(b)) clearly shows an amorphous halo along with the polycrystalline rings of α-Al. The increase in XRD peak width of α-Al with increasing melt-spun wheel velocity (Fig. 1) suggests that its grain size decreases with increase in cooling rate. The grain size of Al, calculated from the full width at half maximum of (111) peak, showed a decrease from 40 to 20 nm with increase in melt-spun wheel velocity from 20 to 50 m/s. It should be noted that the contribution of instrumental broadening and lattice strain to the XRD peak width have not been considered in the present calculation and hence the grain size calculated as above would be smaller than the actual grain size. Figs. 3(a)-(d) show the bright field electron images of the alloy melt-spun at wheel speeds of 20, 30, 40 and 50 m/s, respectively. The figure clearly depicts a continuous decrease in grain size of Al with increase in cooling rate. In the case of the alloy melt-spun at 20 m/s, the bright field image (Fig. 3(a)) is obtained from a region showing very fine *i*-phase particles, so as to reveal the grain size of α-Al. Hence the microstructure differs significantly from that shown in Fig. 2(a), which was taken from a coarse microstructure to identify the phase by the microdiffraction technique. In Fig. 3, the non-uniformity of the contrast within Al grains is due to the inclusions of nanoscale precipitates or amorphous phase as reported earlier in detail.[12] Nanoscale particles of amorphous phase embedded in α-Al grains are clearly seen in the high resolution image (Fig. 4).

The DSC traces of the alloy at different melt-spun wheel velocities are shown in Fig. 5. The alloys containing α-Al and *i*-phase mixture (in the wheel velocity range of 20-40 m/s) showed one exotherm in the temperature range of 765-780 K. Isochronal annealing of these alloys at 873 K in the DSC and subsequent XRD studies have shown the equilibrium phase mixture of $Al_{13}Fe_4$, $Al_{11}V$ and α-Al. In contrast to the above, the alloy containing amorphous phase and α-Al (melt-spun at 50 m/s) showed two broad exothermic peaks at 715 and 760 K and a sharp exotherm at 770 K. Isochronal annealing of this alloy at 723 K in DSC has shown the precipitation of *i*-phase from the amorphous phase as shown in Fig. 6. This suggests that the first broad peak observed in the DSC trace in this sample corresponds to the transformation of the amorphous phase to the *i*-phase. Annealing this sample at higher temperature (873 K) yielded the same equilibrium phase mixture (Fig. 6) as was observed at other wheel velocities.

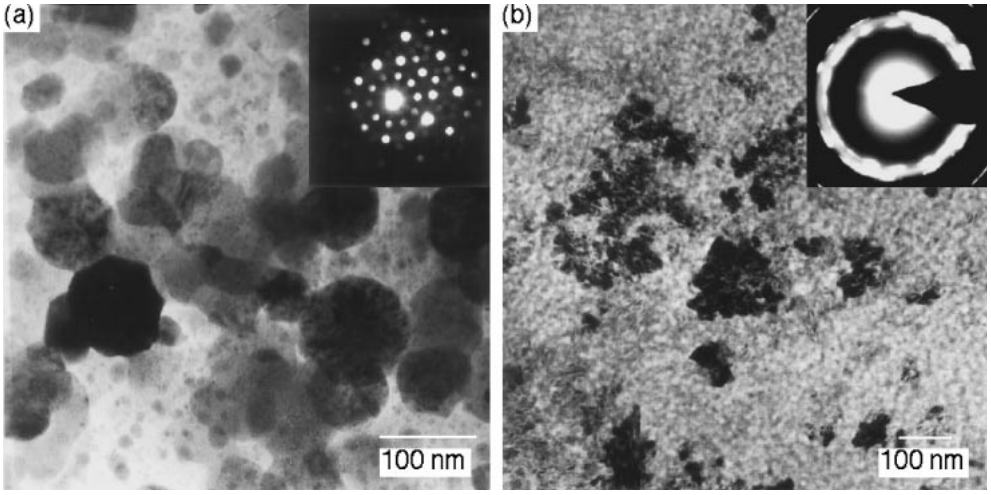

Fig. 2 Bright field TEM images of $Al_{94}V_4Fe_2$ alloy melt-spun at (a) 20 and (b) 50 m/s. The inset of (a) is the microdiffraction pattern obtained from an *i*-phase particle and that of (b) is the selected area diffraction pattern from the alloy melt-spun at 50 m/s.

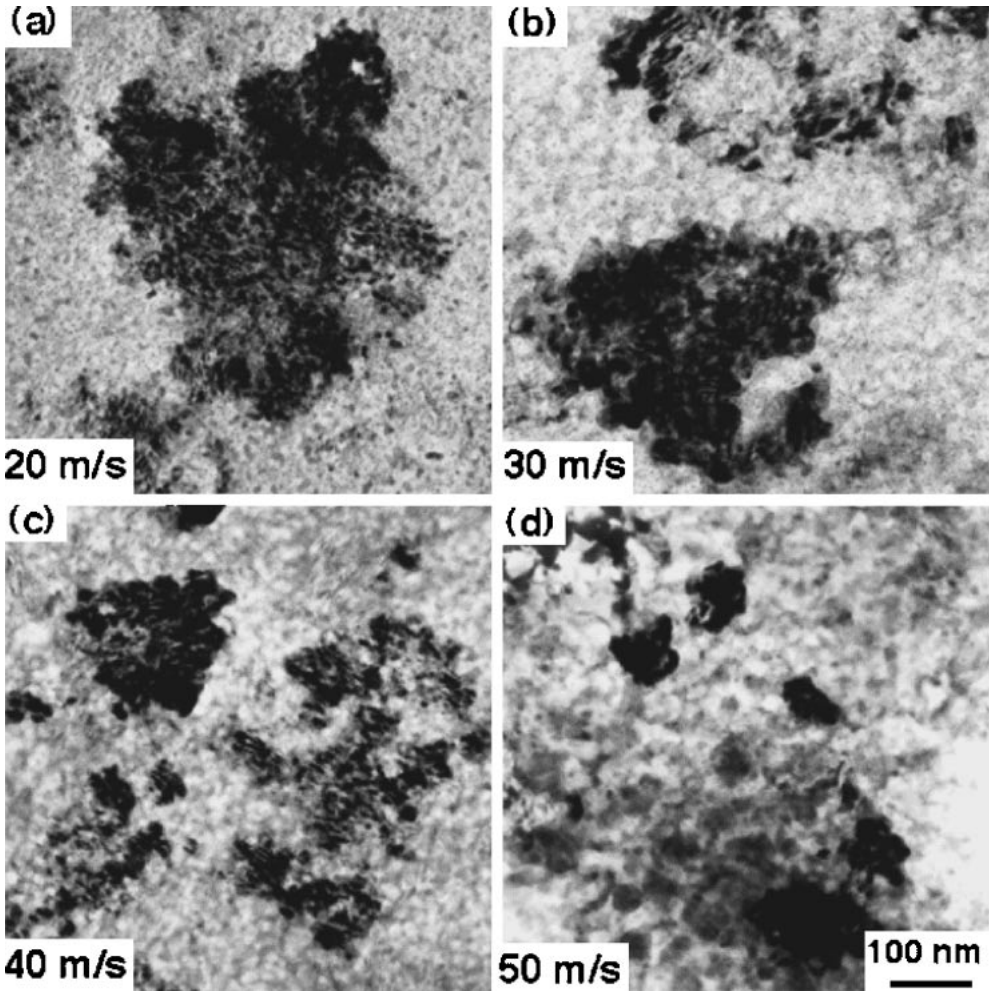

Fig. 3 Bright field TEM images of $Al_{94}V_4Fe_2$ alloy melt-spun at (a) 20, (b) 30, (c) 40 and (d) 50 m/s, showing refinement in the grain size of α-Al.

Figure 7(a) shows the TEM bright field image of the alloy melt-spun at 50 m/s and subsequently isochronally annealed in DSC at 723 K. The microstructure revealed the presence of fine spherical *i*-phase particles in the nanocrystalline α-Al grains. The selected area diffraction pattern (Fig. 7(b)) clearly evidences the replacement of amorphous halo with the sharp diffraction rings corresponding to the *i*-phase between the (111) and (200) rings of α-Al. Figure 7(c) is the micro diffraction pattern obtained from one of the *i*-phase particles in the 5-fold orientation, confirming their quasi-crystalline nature.

In order to identify the composition of the individual phases, the alloy melt-spun at 30 m/s was studied by 3DAP. Figures 8(a) and (b) show the 3DAP map of V and Fe, respectively, in a sample volume of $10 \times 10 \times 65$ nm. Each dot in the elemental map represents one atom. The composition profile of Al, Fe and V in the selected volume of $5 \times 5 \times 25$ nm is shown in Fig. 8(c). Based on the composition profile, the presence of three phases can be clearly delineated as shown in Fig. 8(c). The region, which has the highest amount of Fe and V is the amorphous phase and its composition appears to be close to $Al_{85}Fe_8V_7$. The α-Al region is clear from the depleted solute content and its richness in Al. The region sandwiched between the α-Al and the amorphous phase is the *i*-phase, which could either form by a peritectic reaction between the α-Al and the liquid or directly from the liquid. However, during melt-spinning, the chances of peritectic reaction are less and hence, the latter mechanism is more realistic one. The residual liquid available after the formation of the *i*-phase gets converted to the amorphous phase. The formation of *i*-phase from the amorphous phase is also evident from the isochronal annealing of the alloy melt-spun at 50 m/s in DSC at 723 K. The 3DAP results also showed the presence of small amount of amorphous phase in the alloy melt-spun at 30 m/s, which was not evident from the XRD and conventional TEM studies. From the composition profile, it appears that the *i*-phase is very poor in Fe and is mainly a binary phase with about 15 at% of V in it. This composition is close to the $Al_{11}V_2$ stoichiometry.

The tensile fracture strength of the $Al_{94}V_4Fe_2$ alloy increases with increase in wheel velocity from 20 to 40 m/s, beyond which it decreases slightly as shown in Fig. 9. The values of tensile fracture strength of the alloy at different wheel velocities have been taken from Inoue *et al.*[9] The line passing through the data points in Fig. 9 is a Gaussian fit to the data points. The fitted line suggests that the fracture strength of the alloy reaches a maximum at a wheel velocity close to 40 m/s.

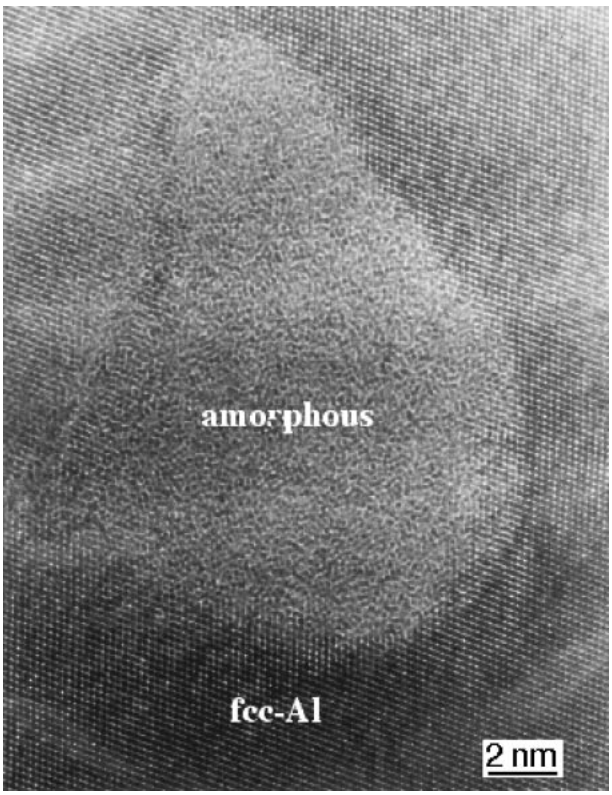

Fig. 4 High resolution electron image of the $Al_{94}V_4Fe_2$ alloy melt-spun at 50 m/s showing embedded amorphous phase in α-Al matrix.

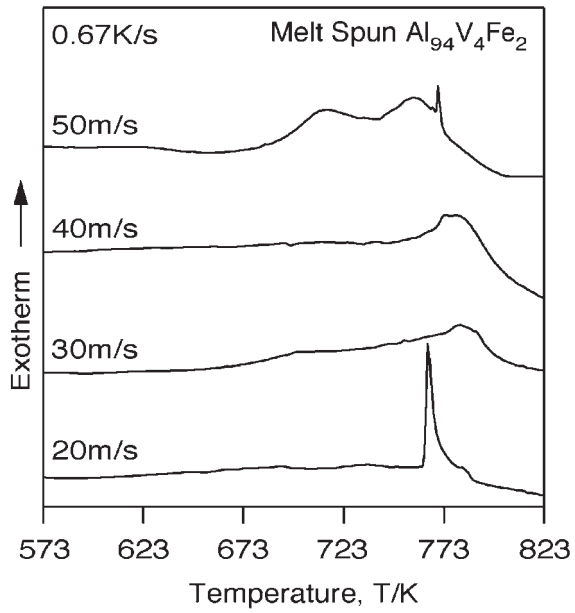

Fig. 5 DSC traces of $Al_{94}V_4Fe_2$ alloy melt-spun in the wheel velocity range of 20-50 m/s.

4. Discussion

The present results indicate that the microstructure of the $Al_{94}V_4Fe_2$ alloy changes from a nanocomposite of fcc α-Al and *i*-phase to that of fcc α-Al and amorphous phase when the melt-spun wheel velocity is increased from 20 to 50 m/s. The alloy remains as a nanocomposite of *i*-phase and α-Al up to 40 m/s. The grain size of α-Al and the particle size of *i*-phase decrease with increase in wheel velocity. At 50 m/s, the alloy is a nanocomposite of α-Al and amorphous phase.

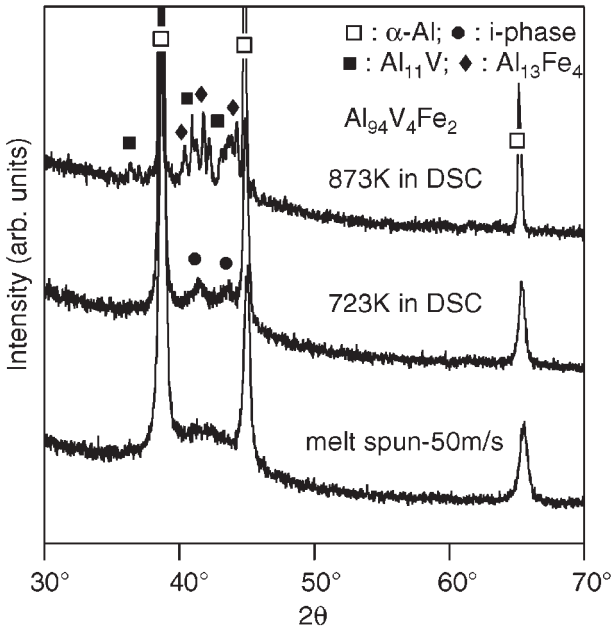

Fig. 6 XRD patterns of $Al_{94}V_4Fe_2$ alloy melt-spun at 50 m/s and subsequently isochronally annealed in DSC at 723 and 873 K.

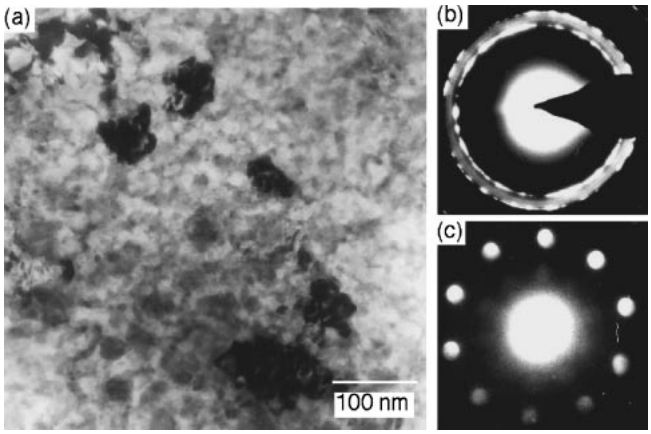

Fig. 7 (a) TEM bright field image of $Al_{94}V_4Fe_2$ alloy melt-spun at 50 m/s and subsequently isochronally annealed in DSC at 723 K. (b) is the selected area electron diffraction pattern from the alloy and (c) is the micro diffraction pattern in the 5-fold orientation from an *i*-phase particle.

The microstructure of the alloy reveals the possible solidification sequence of alloy. It is obvious that α-Al nucleates first during solidification as the composition of the alloy is rich in Al, where the driving force for the nucleation of α-Al is very high. At higher cooling rates, nucleation of α-Al occurs at higher undercooling, leading to a decrease in its grain size with increasing cooling rate. With the nucleation of primary α-Al, the remaining liquid becomes enriched in the solute content, which solidifies either into a crystalline phase, *i*-phase or amorphous phase depending on the cooling rate or the degree of undercooling. From the present results it is clear that melt spinning in the range of wheel velocities of 20-40 m/s, the liquid solidifies as *i*-phase and at 50 m/s, it solidifies as an amorphous phase.

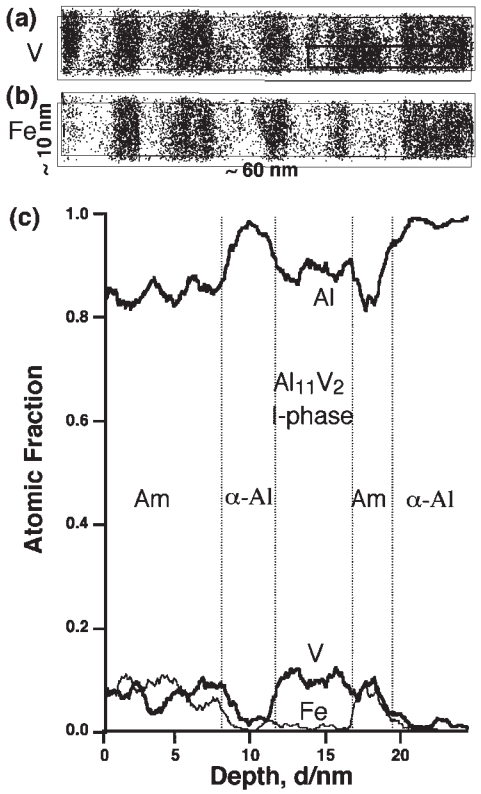

Fig. 8 3DAP elemental mapping of (a) V, (b) Fe and (c) composition profiles of Al, Fe and V in a selected volume in the $Al_{94}V_4Fe_2$ alloy melt-spun at 30 m/s.

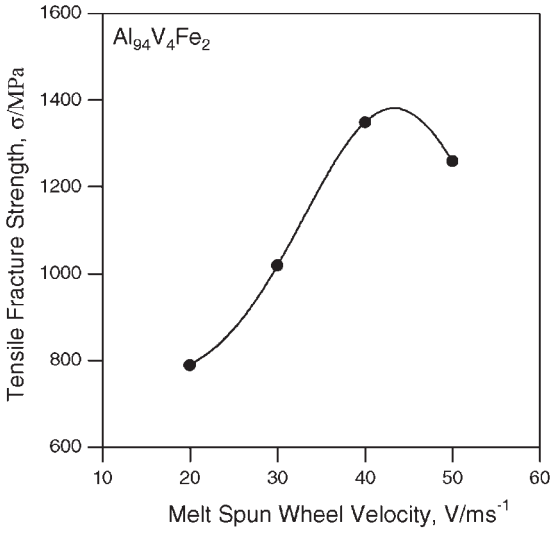

Fig. 9 Tensile fracture strength of $Al_{94}V_4Fe_2$ alloy at different melt-spun wheel velocities.

From the 3DAP studies, it is clear that the *i*-phase is mostly a binary compound of Al and V with the stoichiometry close to $Al_{11}V_2$, where as the amorphous phase contains both the solute elements at levels higher than that observed in the bulk composition of the alloy. This suggests solute partitioning into the amorphous and *i*-phases, leaving the matrix depleted in the solutes. Interestingly, Fe appears to preferentially partition to the amorphous phase instead of the *i*-phase. Hono *et al.*[12] also reported enrichment of V and Fe in the amorphous phase. Although only amorphous phase was identified in their sample by TEM, they observed compositionally three distinct regions by APFIM, α-Al, Al-12V, and Al-12V-10Fe (at%). They interpreted both the Al-12V and Al-12V-10Fe regions as amorphous phase. Since Al-12V is close to the composition of the *i*-phase, as identified in this study, it is possible that the binary amorphous phase transforms to the *i*-phase after annealing or at a slower cooling rate.

The tensile fracture strength of the alloy reaches a maximum at a melt-spun wheel velocity close to 40 m/s. It is important to note that the tensile fracture strength of the alloy reaches close to 1.4 GPa, which is exceptionally high for any Al based alloy. Thus, the present results confirm the earlier reports of Inoue[1] that the tensile strength of Al alloys can reach the GPa regime when the alloy is made into a nanocomposite of α-Al, *i*-phase or amorphous phase. The correlation of the mechanical properties with the microstructure observed in the present study indicates that the significant increase in the strength with increase in cooling rate up to 40 m/s can be mainly attributed to the refinement of α-Al grains and the presence of nanocrystalline *i*-phase. Thus, the highest strength values appear to be obtained when the microstructure is a nanocomposite of α-Al and *i*-phase. The replacement of *i*-phase with the amorphous phase at higher cooling rate decreases the strength of the alloy, in spite of the further decrease in the grain size of α-Al, which is expected to increase the strength further. This observation is in contrast to that made by Inoue[1] that the maximum strength is achieved when the microstructure consists of a nanocomposite of α-Al and amorphous phase.

The exceptionally high tensile fracture strength observed for the nanocomposite structure in the alloy studied could be mainly due to three factors, namely, (a) nanocrystalline structure of α-Al leading to Hall-Petch type strengthening, (b) precipitation strengthening due to nanocrystalline *i*-phase (or amorphous) particles in the nanocrystalline Al matrix and (c) solid solution strengthening due to the solute elements. While the first two factors are clearly evident from the microstructural studies, the third factor was evident from a careful observation of the XRD patterns of the alloy melt-spun at different wheel velocities. A systematic shift of the α-Al peaks to higher angles was observed with increase in melt-spun wheel velocity (Fig. 1), indicating a continuous decrease in the lattice parameter. The lattice parameter calculated from the shift in the (111) peak of α-Al decreased from 0.40407 to 0.40206 nm with increase in melt-spun wheel velocity from 20 to 50 m/s. The lattice parameter of pure Al is 0.40494 nm. The decrease in lattice parameter of α-Al with increase in cooling rate suggests greater supersaturation of Al with Fe and V. It is important to note that the atomic radii of both Fe and V (0.124 and 0.131 nm, respectively) are lower than that of Al (0.143 nm) and hence dissolution of Fe and V in Al are expected to lower the lattice parameter of the latter. Sasaki *et al.*[15] have earlier reported solid solution strengthening in nanocrystalline Al-Fe alloys leading to strength levels of the order of 1 GPa with about 2.5 at%Fe. In the light of the above, the present results are not surprising and demonstrate the design criteria necessary to develop high strength Al alloys.

5. Conclusions

(1) The microstructure of the high strength $Al_{94}V_4Fe_2$ alloy consists of a nanocomposite of α-Al and *i*-phase in the melt-spun wheel velocity range of 20-40 m/s. At 50 m/s, the alloy shows a nanocomposite of α-Al and amorphous phase.
(2) Nanoquasicrystallization is the first stage of crystallization of the amorphous phase obtained at 50 m/s.
(3) The highest strength for the alloy is achieved when the alloy is a nanocomposite of α-Al and *i*-phase.
(4) The 3DAP studies indicate that the *i*-phase has a stoichiometry of $Al_{11}V_2$ and the composition of the amorphous phase is close to $Al_{85}Fe_8V_7$.

REFERENCES

1) A. Inoue: Prog. Mater. Sci. **43** (1998) 365-520.
2) H. Chen, Y. He, G. J. Shiflet and S.J. Poon: Scr. Mater. **25** (1991) 1421-1424.
3) S. K. Das and L. A. Davies: Mater. Sci. Eng. **98** (1988) 1-12.
4) Y. H. Kim, A. Inoue and T. Masumoto: Mater. Trans., JIM **31** (1990) 747-749.
5) Y. H. Kim, A. Inoue and T. Masumoto: Mater. Trans., JIM **32** (1991) 331-338.
6) A. Inoue M. Watanabe, H. M. Kimura, F. Takahashi, A. Nagata and T. Masumoto: Mater. Trans., JIM **33** (1992) 723-729.
7) A. Inoue: Mater. Sci. Eng. **A179/180** (1994) 57-61.
8) H. M. Kimura, A. Inoue, K. Sasamori, K. Kita and T. Oogi: J. Jpn. Inst. Light Met. **48** (1998) 494-500.
9) A. Inoue, H. Kimura, K. Sasamori and T. Masumoto: Mater. Trans., JIM **36** (1995) 1219-1228.
10) A. Inoue, H. Kimura, K. Sasamori and T. Masumoto: Mater. Trans., JIM **37** (1996) 1287-1292.
11) A. Inoue, H. Kimura, K. Sasamori and T. Masumoto: Nanostructured Mater. **7** (1996) 363-382.
12) K. Hono, Y. Zhang, T. Sakurai and A. Inoue: Mater. Sci. Eng. **A250** (1998) 152-157.
13) E. S. Humphreys, P. J. Warren and A. Cerezo: Mater. Sci. Eng. **A250** (1998) 158-163.
14) B. Deconihout, L. Renaud, G. Da Costa, M. Bouet, A. Bostel and D. Blavette: Ultramicroscopy **73** (1998) 253-260.
15) H. Sasaki, K. Kita, J. Nagahora and A. Inoue: Mater. Trans. **42** (2001) 1561-1565.